Chapter 2

ZnO Nanowire Growth on Porous Silicon

2-1 Porous Silicon Formation and Application

Porous silicon (PS) has the morphology composed by a disordered web of pores. Its structure is like a sponge where quantum effects play a fundamental role, i.e. PS could be viewed as a quantum sponge, and as a sponge it can be permeated by a variety of chemicals and its enormous internal surface rules its properties. These features made PS lots of applications such as light emitting diodes or high reactivity of sensors.

PS has opened new possibilities for Si based integrated circuits due to its fascinating optical and electronic properties. Applications such as visible photoluminescence at room temperature, highly efficient electroluminescent devices (ELDs) and photodetectors have been reported previously. [129]- [131] PS also looks promising for use in biological and chemical sensing devices. [132] Recently, PS has been selectively patterned by e-beam lithography, [133] enabling the deposition of well-aligned carbon nanotubes on Si substrates. [134] Furthermore, PS can be easily obtained, and the chemical etching process used would ideally be compatible with established technologies for fabricating Si-based devices. Even though the interest in PS renewed after the observation of its emission properties, the potential application areas of PS are much wider than simple light emission. In Table 2, a list is presented.

Application area	Role of PS	Key property
Optoelectronics	LED	Efficient electroluminescence
	Waveguide	Tunability of refractive index
	Field emitter	Hot carrier emission
	Optical memory	Non-linear properties
Micro-optics	Fabry–Perot filters	Refractive index modulation
	Photonic band gap structures	Regular macropore array
	All optical switching	Highly non-linear properties
Energy conversion	Antireflection coatings	Low refractive index
	Photoelectrochemical cells	Photocorrosion cells
Environmental monitoring	Gas sensing	Ambient sensitive properties
Microelectronics	Micro-capacitor	High specific surface area
	Insulator layer	High resistance
	Low-**k** material	Electrical properties
Wafer technology	Buffer layer in heteroepitaxy	Variable lattice parameter
	SOI wafers	High etch selectivity
Micromachining	Thick sacrificial layer	Highly controllable etching parameters
Biotechnology	Tissue bonding	Tunable chemical reactivity
	Biosensors	Enzyme immobilization

Table 2 Potential application areas of PS [135]

PS is formed by an electrochemical etching of Si in an HF solution. Following an electrochemical reaction occurring at the Si surface a partial dissolution of Si settles in. There are various factors which rule this process.

PS was performed using only HF diluted in deionized and ultra-pure water. Absolute ethanol is usually added to the aqueous solution to increase the wettability of the PS surface and to infiltrate the pores. This is very important for the lateral homogeneity and the uniformity of the PS layer in depth. Moreover, it has been found that lateral inhomogeneity and surface roughness can be reduced, increasing electrolyte viscosity, either by diminishing the temperature or introducing glycerol to the composition of the HF solution.

The electrochemical cell is a Teflon beaker shown in Fig. 5. The Si wafer acts as the anode and the cathode is generally made of platinum. Using this cell PS is formed all over the wafer surface exposed to HF, including the cleaved edges.

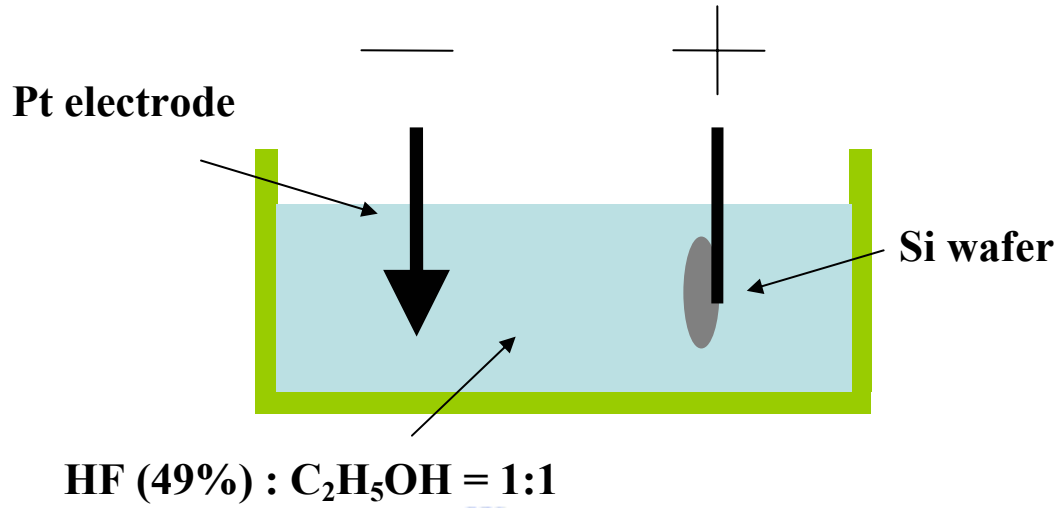

Fig. 5 anodization cell and for PS formation

Si atiom was ionized by the HF and the chemical reaction formula was as following:

$$Si_{(s)}+6HF_{(aq)}+2h^{+}\rightarrow H_2SiF_{6\,(aq)}+H_2+2H^{+}_{(aq)} \qquad (2\text{-}1)$$

In Fig. 6, the surface morphology (6a) and the cross section (6b) images of PS are shown. The electric current is 40mA and the etching time is 10 secs. We used P+ Si wafer with resistivity ~0.02Ωcm. Nanoscale etching path and large surface roughness can be seen.

In this study, we demonstrate the feasibility of growing single crystalline ZnO nanorods on PS without any catalyst. The growth and characterization of a single ZnO nanorod are also demonstrated in detail. Moreover, the probable growth mechanism of ZnO nanorods on the PS surface is examined.

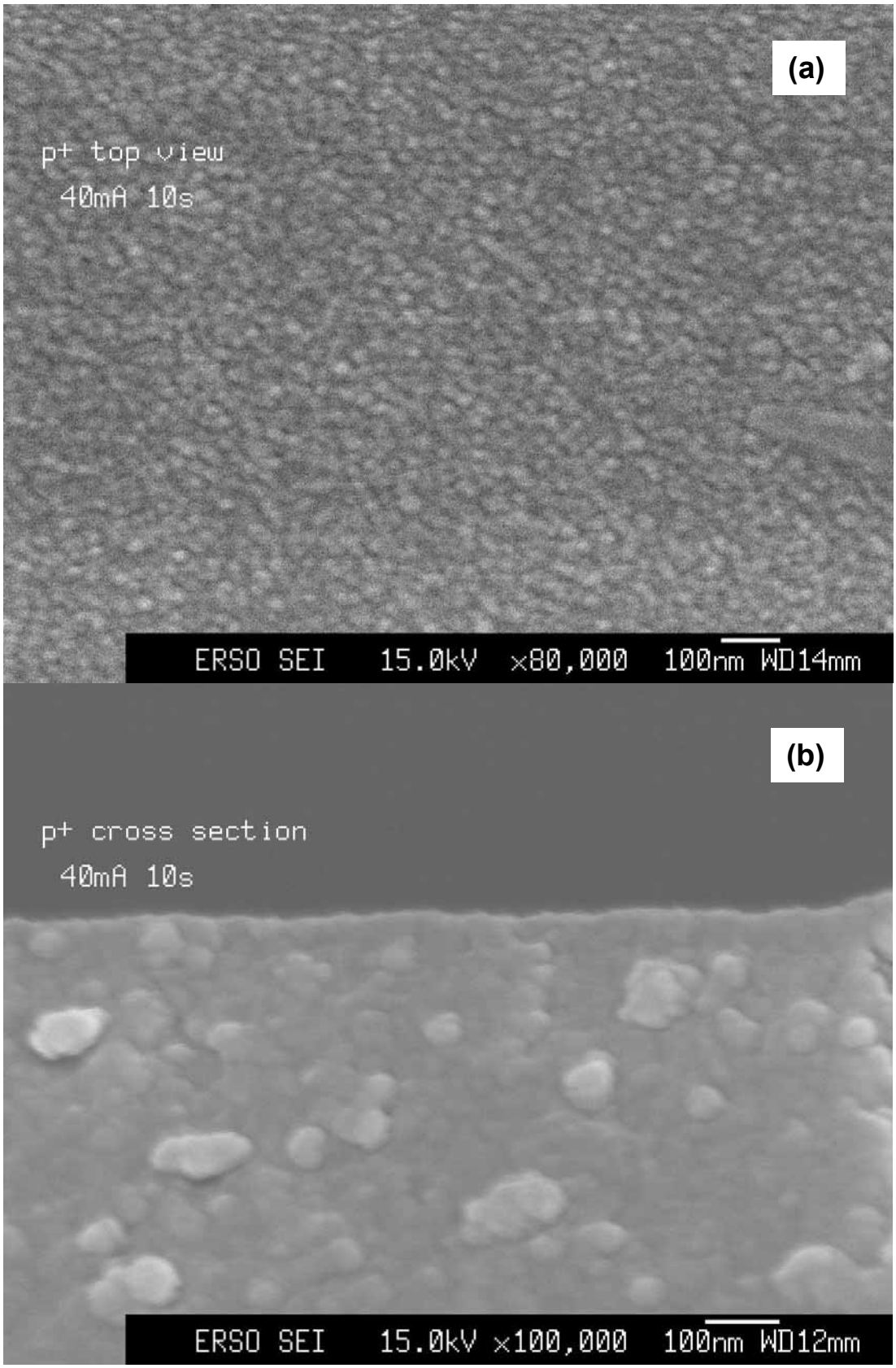

Fig. 6 The SEM images of PS : the surface morphology (a) and the cross section (b).

2-2 Growth techniques of ZnO nanorods

Numerous technologies have been developed to grow ZnO nanorods on different substrate materials, which include the vapor-liquid-solid (VLS) method for growth on sapphire with Au as the catalyst [136], electrodeposition for growth on anodic alumina membrane (AAM) templates [137]and the vapor-solid (VS) method without a catalyst for growth on Si [138]-[139].

The primary vapour based nanorod growth technique is the vapour-liquid-solid (VLS) process first reported by Wagner et al. [140] during his studies of large single-crystalline whisker growth. As the name of the growth technique suggests, the growth agent undergoes a transformation from a vapour form, to a liquid form, and finally to a solid form as the nanorod. Various methods have been developed in synthesizing ZnO nanorods [141]-[147]. Previous effort in synthesis of high-quality ZnO nanorods had employed high-temperature process such as vapor–liquid–solid (VLS) mechanism, in which a metal liquid droplet acts as an active catalyst [148]. In this method, the growth temperature was maintained beyond 800^{o}C and the nanorods were randomly grown on substrates. However, to establish an applicable process for the integrated photonic devices, one may have to develop a relatively low temperature and selective growth method for growing desired structures on the patterned templates.

The formation of ZnO nanorods includes two steps: nucleation and growth. For the conventional VLS process, metal catalyst such as gold is necessary to form the liquid metal – alloy droplets and the nanorods are grown through condensation of the source metal from the supersaturated liquid metal – alloy droplets

followed by immediate oxidation.

However, if there are no metal catalysts involved in the growth process, no droplets were found at the ends of nanorods, which is the main feature of the VLS mechanism, the growth mechanism is not based on VLS but it is likely governed by vapor–solid process [149] or the so-called self-catalyzed VLS process [150]. ZnO buffer layer may provide nuclear seeds for the thermally evaporized Zn atoms to condense onto the substrate [151]. Thus, the already condensed Zn not only acts as the seed but also provides an energetically favorite site for adsorption of oxygen. It has been demonstrated that the morphology of the crystals is related to the relative growth rates of various crystal faces that bound the crystal; these growth rates are not only determined by the internal structure of the crystal but also affected by the growth conditions [152]. Table 3 showed the difference of the two mechanisms.

	VLS	VS
Catalyst	Au, Fe, Co, Ni, Zn	None
Temperature	High 650C	Low 450C
Seed	Metal droplet Au, Zn	Substrate morphology
Theory	Phase diagram Au/Zn alloy	Nucleation and growth theory
Reaction	Chemical	Physical
Concentration	Composition Alloy fixed	Wetting layer changable

Table 3 VLS and VS mechanism analysis

The rough morphology of a PS surface was proven advantageous for the growth of nanorods by reducing its strain [138] and increasing the number of nuclei sites [153]. We have demonstrated the possibility of selective growth of ZnO nanorods on a low temperature without any catalyst. The vapor–solid mechanism might be responsible for this selective growth of the ZnO nanorods. This low temperature growth technique not only provides a convenient way to grow 1D-ZnO in large-area but also opens up an opportunity for fabricating ZnO nanorod -based devices.

First, the PS substrate was fabricated by anodizing a p-type Si wafer (resistivity ~0.02Ωcm) in a solution (49% HF: ethanol=1:1) at a current density of 500mA/cm2 for 1min. After anodization, the PS substrate was cleaned with DI water. Prior to the growth of ZnO, PS samples were dipped in a HF solution to remove the native oxide. Then, the ZnO nanostructures were fabricated on PS by thermal evaporation without any catalyst. A cleaned p-type Si wafer was placed near PS for comparison with the growth under different surface conditions. The synthesis was carried out in a quartz tube (diameter 28mm, length 1m) with mixed pure ZnO powders and carbon powders (weight ratio 1:1) as source materials. The quartz tube was then placed in a horizontal furnace as shown in Fig. 7. The temperature at the source position, the middle part of the quartz tube, was set at 950 ℃.The temperature along the tube was gradually lowered to about 600℃ at which the PS substrate was placed. During evaporation, Ar flowed as a carrier gas inside the quartz tube. The gas flow was kept at 150 sccm and the pressure was maintained at 10 torr. After evaporation for 4 hr, gray products on the PS surface but not on the other silicon wafer, were found. The morphologies and microstructures of the products were investigated by field-emission

scanning electron microscopy (FESEM), transmission electron microscopy (TEM), energy dispersive X-ray (EDX), and grazing-angle X-ray diffraction (XRD). A photoluminescence (PL) measurement was also performed at room temperature using a He-Cd laser (325nm) as the excitation source.

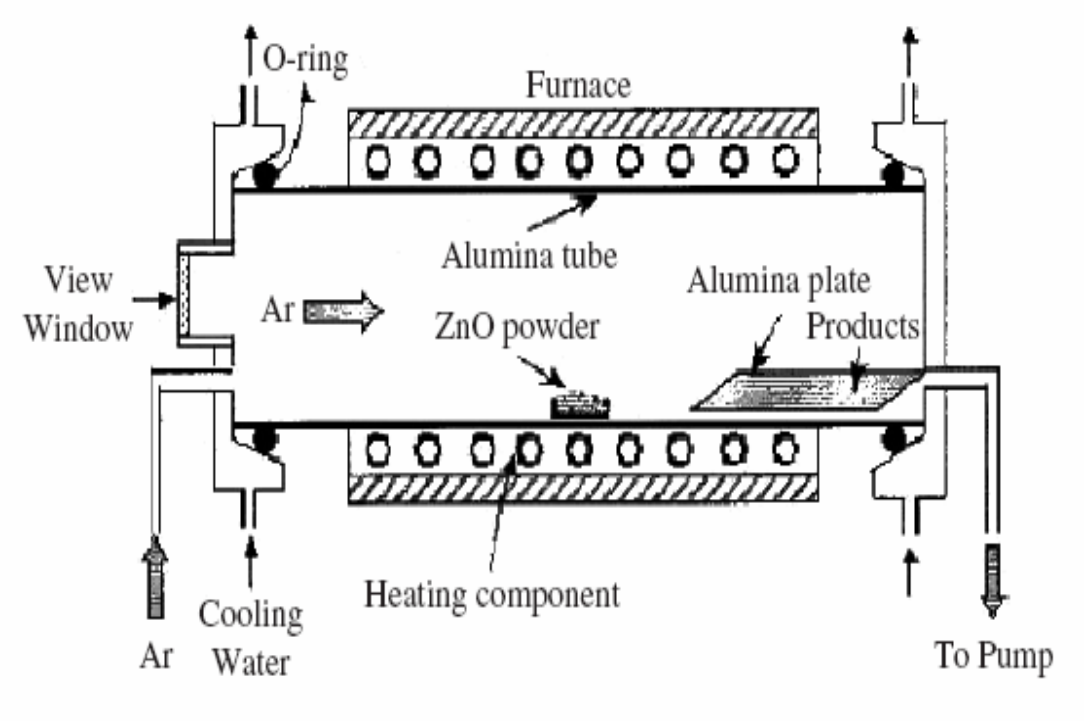

Fig. 7 The facility for grow ZnO nanorods

2-3 Result Analysis and Discussion

Figure 8(a) shows the product grown on the PS substrate by FESEM. The surface morphology showed that the nanorods had grown uniformly. The lengths of all of the nanorods were 2~3um. However, a wetting layer was formed under these nanorods, and the direction of the nanowires depended on the morphology of this wetting layer. As shown in the highly magnified image in Fig. 8(b); the diameter at the base of the nanorods was slightly larger than that at the top. The average diameters of these nanorods were about 70~110nm.

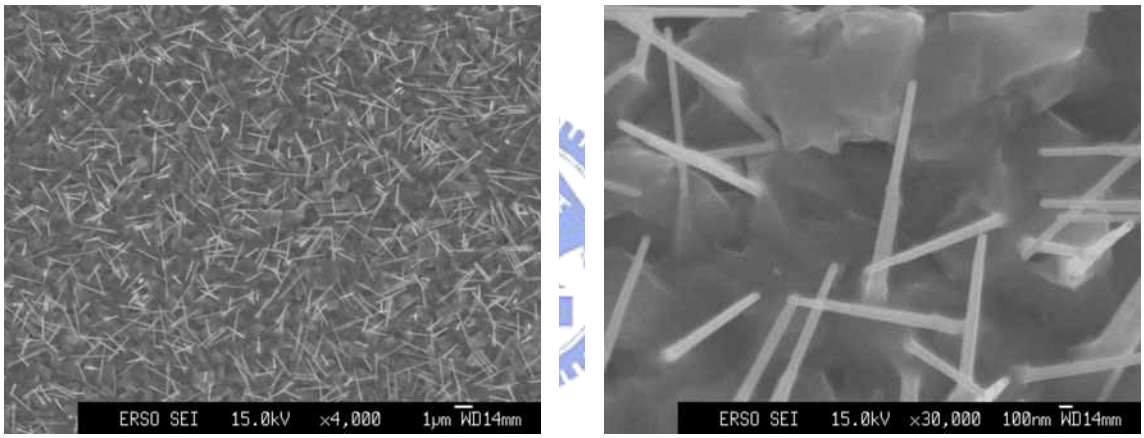

Fig. 8 (a) SEM image of nanorods grown on porous Si substrate. (b) higher magnification of the SEM image. The nanorod diameter at the base was larger than that at the top.

Figure 9 presents the grazing-angle XRD pattern of the product, the wetting layer and the nanowires, which were grown on the surface of the PS substrate. The positions of the peaks in the grazing-angle XRD pattern were consistent with those of the hexagonal structure of bulk ZnO with lattice constants a_o=3.32489Å and c_o=5.2062Å [137]. However, an additional diffraction peak associated with element Zn was observed in this pattern. The position of this peak was found to

be the same as that reported for ZnO nanorods embedded in alumina templates [136]. The product was thus determined to include not only hexagonal ZnO but also element Zn on the surface of the PS substrate.

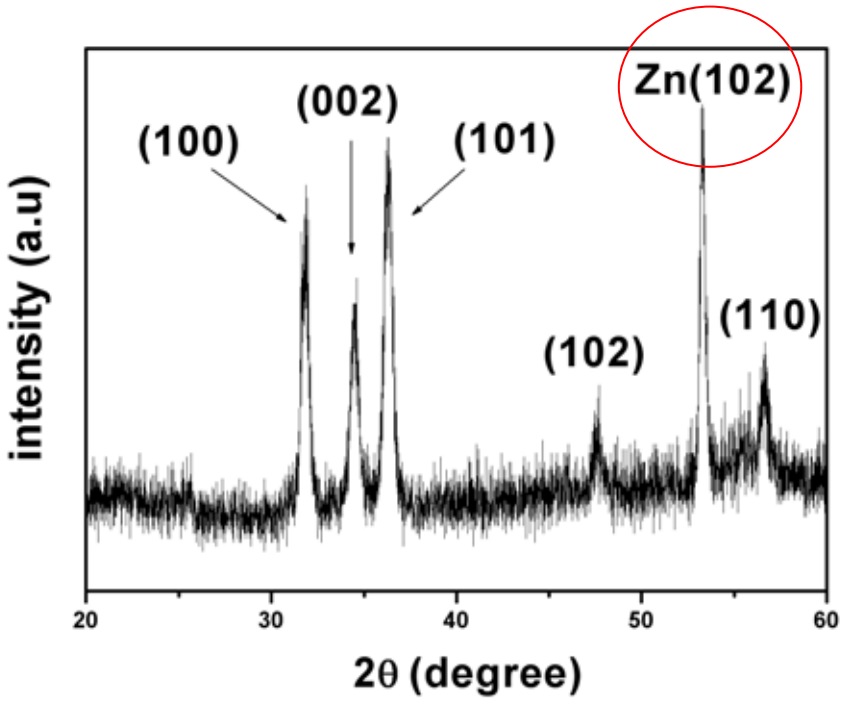

Fig. 9 Both ZnO and Zn existed in the grazing-angle XRD patterns of ZnO nanowires on a PS substrate.

The microstructure of a single ZnO nanowire was examined by TEM. Notably, the observed region was near the top of this single nanorod. Figure 10(a) shows the typical morphology of one ZnO nanorod. The ZnO nanorod consisted of a single crystalline hexagonal structure (wurtzite), which was determined using the selected-area electron diffraction (SAED) pattern shown in the inset. These surprising data seem to be inconsistent with the grazing-angle XRD pattern. We suggest that the top and base of the ZnO nanorod may perform differently. A high-resolution TEM (HRTEM) measurement was carried out to clarify in detail the structure at the top of the nanorod.

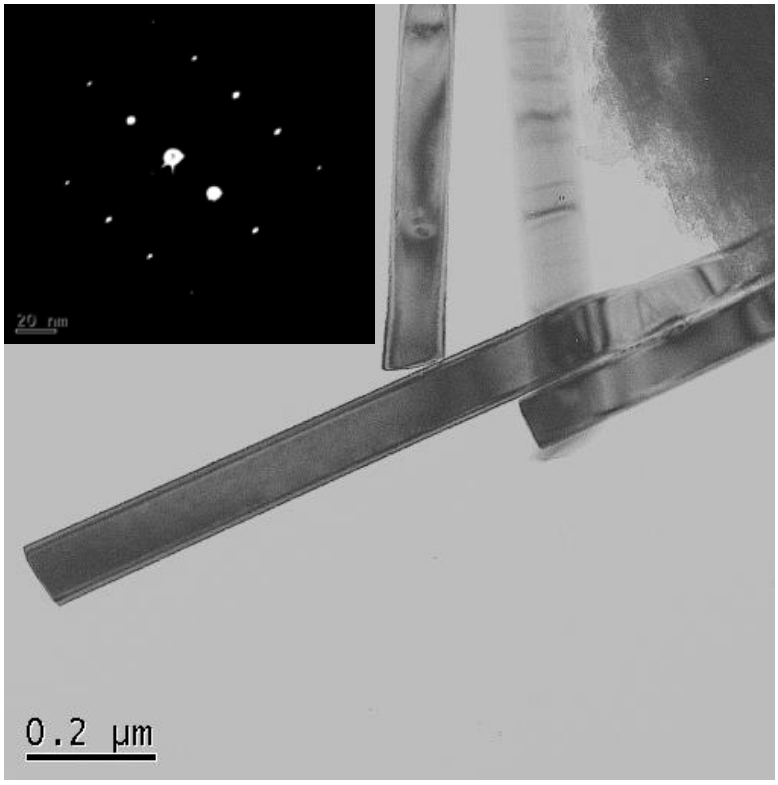

Fig. 10 (a) TEM image of single crystalline ZnO nanorod. SAED patterns are inserted

In Fig. 10(b), the crystalline structure of the single nanorod was identified by high-resolution TEM (HRTEM). A good crystalline structure was obtained, and nearly no defects, such as dislocations and stacking faults, were observed. A very clear lattice fringe was observed between two (002) crystalline planes with a separation of 2.7Å, which is in good agreement with that in ref. [154]. Hence, we positively suggest that the single crystalline structure was formed at the top of the nanorods.

However, a question remains about the diffracted peaks of the polycrystalline structure and the Zn element in the grazing-angle XRD spectra. EDX was therefore used to explain the inconsistency between them.

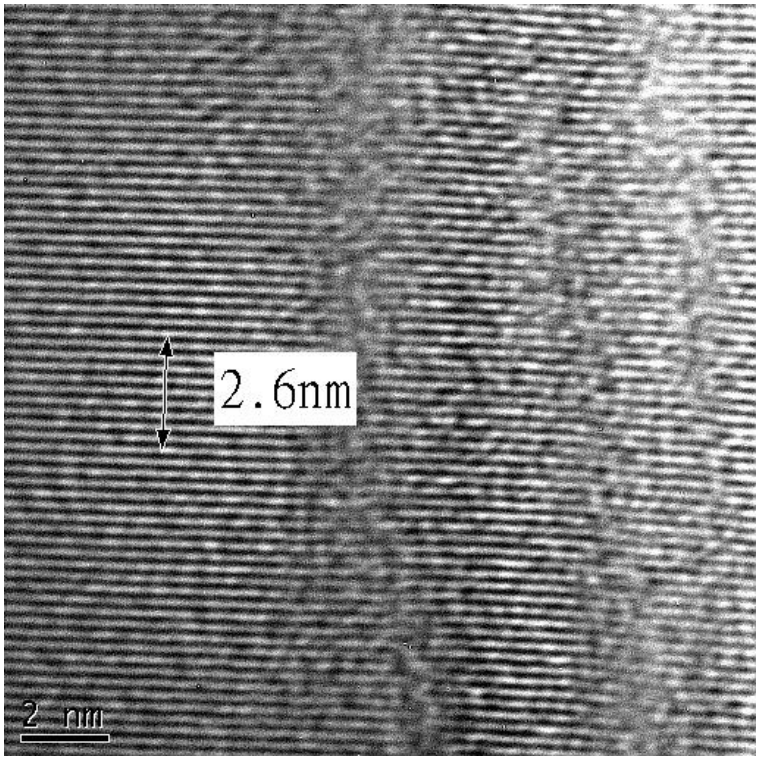

Fig. 10 (b) High-resolution TEM (HRTEM) image of single ZnO nanowire. The d-spacing between two (002) crystalline planes was about 2.7Å.

Figure 11 indicates the EDX spectrum from the base (B) and top (T) of one single ZnO nanorod. Zn yielded three peaks, named, Kα, Lα and Kβ and oxygen yielded another Kα peak. The EDX spectrum from the top of the nanowire was similar to that in a previously reported document [154]. The peak intensity of oxygen at the top of the nanowire was stronger than that at the base, implying an increased atomic ratio of O to Zn. Hence, the concentration of the Zn greatly exceeded that of O at the base of the nanorod. The oxygen concentration increased as the nanowire grew. However, the two peaks, Kα and Kβ from Zn, gradually became weaker at the top than at the base. Accordingly, the EDX results reveal that the difference in the atomic ratio of Zn to O between these two parts of the nanorod yields different bonding structures. The concentration of Zn at the

base of the nanorod was much higher than that at the top, so the base and the underlying wetting layer may have a polycrystalline structure, which is consistent with the results from grazing-angle XRD. Hence, literature[139], [155] and our observations reveal that the vapors of Zn and Zn suboxides initially formed a wetting layer, and then their rough surfaces at the etch pits and hillocks acted as new nuclei sites for nanorods. Therefore, a higher concentration of Zn than that of O is present at the base, which explains the observed coexistence of Zn and ZnO and the finding that the concentration of Zn greatly exceeds that of O in the early stage of formation of the ZnO nanorod according to the grazing-angle XRD and EDX data. Proceeding to this growth process, the adsorption of oxygen and the diffusion of Zn oxides continue at the tips of the ZnO nanowires. Further oxidation increases the concentration of oxygen in the nanorods, improving the quality of ZnO at the top. Therefore, the top of the ZnO nanorods has a single crystalline structure, which is consistent with the TEM pattern. Figure 12 shows the PL spectra of the ZnO nanowires at room temperature. The main emitting bands, a strong ultraviolet (UV) emission at around 380 nm and a weak green emission near 500 nm are observed. The appearance of a strong UV peak is due to the near band edge emission of the wide band gap of ZnO. The green emission can be ascribed to singly ionized oxygen vacancies in ZnO[154] , which is consistent with the observed EDX data obtained here.

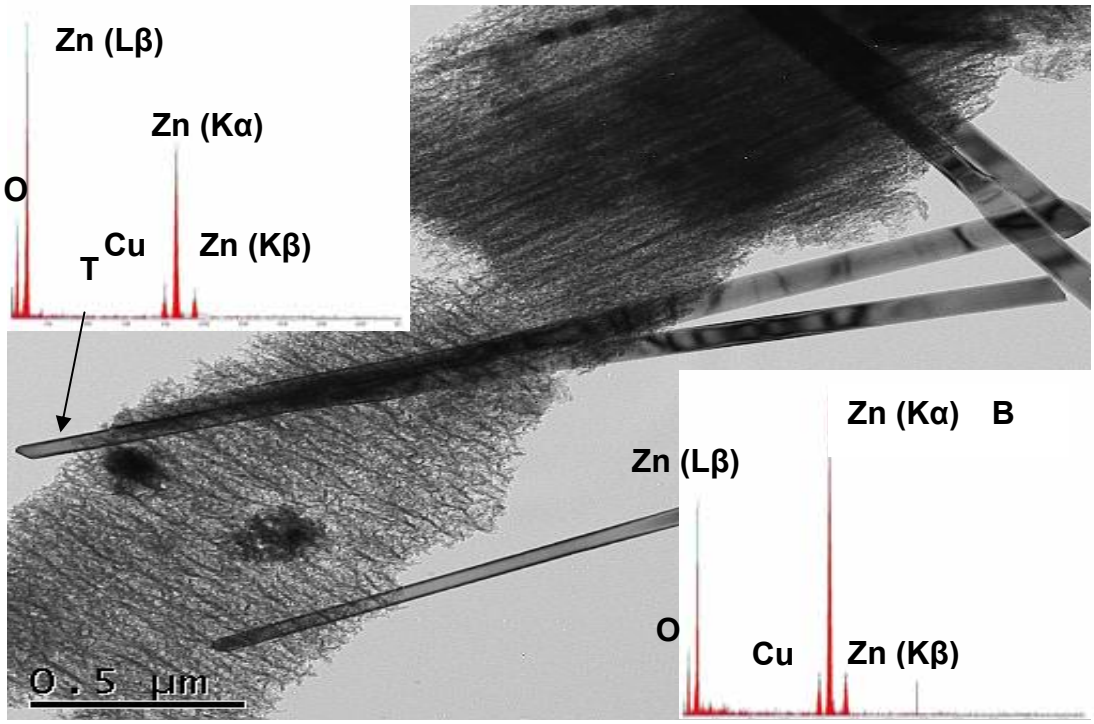

Fig. 11 Micro-EDX spectrum from the base (B) and top (T) of one single ZnO nanorod

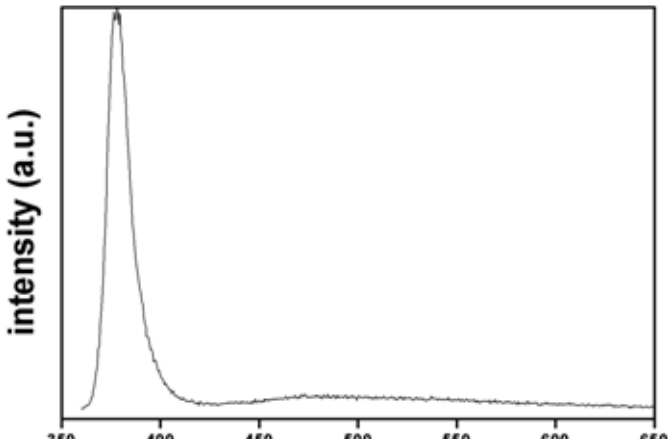

Fig. 12 Photoluminescence spectra of ZnO nanorods on PS substrate recorded at room temperature.

A ZnO wetting layer can easily form on the PS surface. The rough surface morphology of the PS substrate plays a major role in controlling the growth of the wetting layer. The PS surface provides adsorption sites from its etch pits. The wetting layer observed on the surface of porous silicon can be formed from the competition between the expansion due to a decrease in surface energy and contraction due to attraction by dispersive forces in very small cavities[156] .Then, the anisotropy of the polycrystalline wetting layer continuously influences the growth in at least two important ways. First, it can induce an anisotropic strain, thus confining the diffusion of adatoms to one dimension [138]. Second, it generates two types of nucleation site to produce nanorods [157] nanoscale etch pits/hillocks and[158] nanocrystallites[159] .

In this experiment, the ZnO powder was the reagent and was reduced by carbon. A high Zn vapor concentration can result in vapor supersaturation at the beginning of the process due to a high concentration of fresh carbon. The reduced Zn vapor can therefore easily condense on the rough PS surface to form a polycrystalline wetting layer which can provide an anisotropic surface with two types of adsorption site namely, its etch pits and hillocks. A ZnO nanorod was formed by the oxidation of zinc vapor. In this process, the nucleation site critically defines the position and direction of the nanowire when the supersaturation is appropriately controlled. The diameter of the nanowire was also determined by the initial radii of the ZnO polycrystals at the edge or the hillock on the surface of the wetting layer, as shown in Fig. 9.

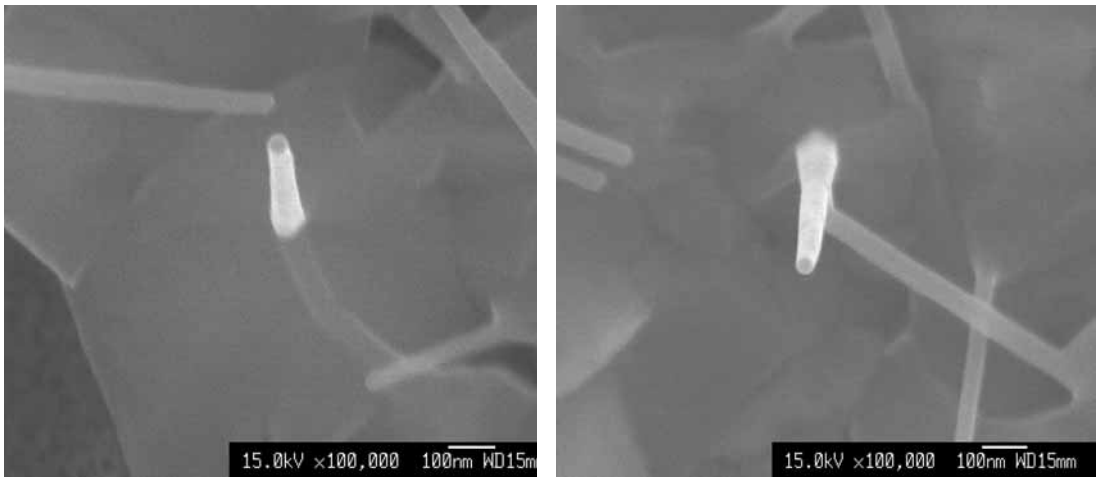

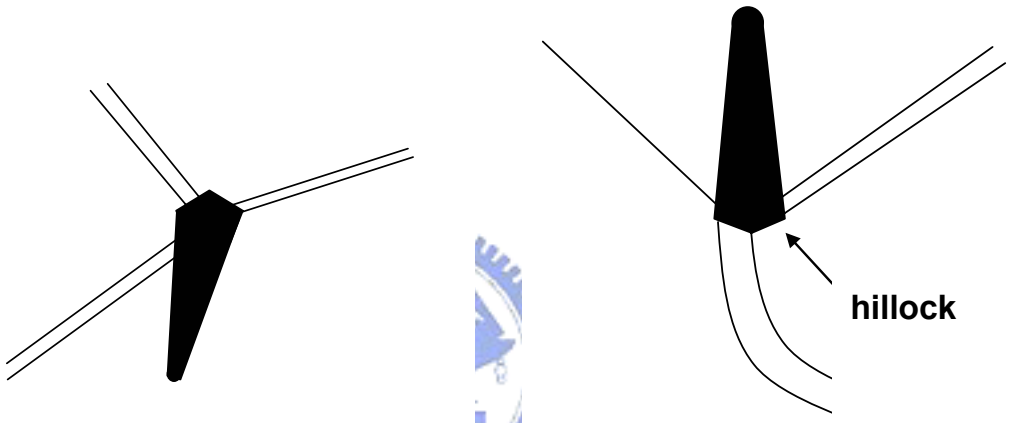

Fig 13. Nanorod grown on hillock of wetting layer to reduce surface energy.

When the nanowire began to grow, the polycrystalline wetting layer caused the crystals to grow in various crystalline directions. Therefore, the diameter was larger at the base of the nanowire. As the nanowire lengthened, the crystals grew quickly from the [001] direction to form a flat plane, reducing the surface energy. Thus, the other facets of the ZnO nanowires gradually disappeared [155] . Consequently, ZnO nanowires with flattened surfaces and smaller diameters were formed.

We have also investigated the growth mechanism of the ZnO nanowires formed on the PS substrate. The synthesis was based on the thermal evaporation of ZnO powders under controlled conditions without a catalyst. As a result, the mechanism differs from that of the growth of ZnO nanowires with a metal catalyst called the vapor-liquid-solid (VLS) process. Furthermore, Hu et al. and Yao et al. proposed another model called the self-catalyzed VLS growth model[160] - [161]. They suggested that the vaporized Zn is deposited in the form of a liquid droplet. Liquidized zinc serves as a seed for the growth of ZnO whiskers. The Zn droplets then react with oxygen to form ZnO, so the formation of ZnO on the Zn liquidized droplets is similar to the VLS mechanism. Here, Zn not only acts as the reactant but also provides an energetically favored site for the adsorption of oxygen. Accordingly, it requires no additional transition metal as a catalyst. It should be noted that nanowires would grow when a catalyst is presented in the two mechanisms. However, in our present work, a wetting layer with excess Zn and ZnO polycrystalline structures were formed on the PS surface as revealed by the EDX and grazing-angle XRD measurements. Although the wetting layer had everywhere a high concentration of Zn, nanowires could only be found at the edge or hillock surrounding the surface of the wetting layer as shown in FESEM. Therefore, we consider the growth mechanism is not similar to the growth of ZnO with a metal catalyst or self-catalyzed VLS mechanism. Instead, the growth may have proceeded in a vapor-solid (VS) process.

2-4 Conclusion and Application

PS technology is, for the first time, used to grow ZnO nanorods on the surface of a PS substrate with a rough orphology without any catalyst. The characteristics of these nanorods were investigated by FESEM, TEM, EDX, grazing -angle XRD and PL measurements. The PS surface provides a rough surface morphology, Zn vapor might condense easily on the PS surface and forms a wetting layer, but not on the flat Si surface, to form a wetting layer by decreasing the surface energy so that ZnO nanorods can grow without any catalyst. The probable growth mechanism should be the VS process.

After Zn vapor condensed, a wetting layer yielding an anisotropic surface was formed, resulting in the formation of new nucleation sites in the nanorods. As the growth continued, the concentration of oxygen increased and the quality of crystalline ZnO nanowires was improved. And the two mechanisms, VS and self-VLS process, might be competed or coexisted.The Zn-rich composition might be different during growth.

In principle, This PS technology is advantageous for growing ZnO nanorods on selected regions because of the rough surface morphology, and therefore, this process can easily be applied for integration with other silicon optoelectronic devices.